Experimental and theoretical charge density of hydrated cupric acetate

Federica Bertolotti, Alessandra Forni, Giuliana Gervasio, Domenica Marabello, Eliano Diana
Experimental and theoretical charge density of hydrated cupric acetate
Polyhedron (2012) 42
DOI: http://dx.doi.org/10.1016/j.poly.2012.05.005

Experimental and theoretical charge density of hydrated cupric acetate

Federica Bertolotti [a], Alessandra Forni [b], Giuliana Gervasio [a], Domenica Marabello [a], Eliano Diana [a]

[a] Dipartimento di Chimica and Centro interdipartimentale di Cristallografia Diffrattometrica (CrisDi), University of Turin, 10125 Turin, Italy [b] CNR-ISTM, Institute of Molecular Sciences and Technologies, University of Milan, Via Golgi 19, I-20133 Milan, Italy

a b s t r a c t

The charge density of the hydrated cupric acetate $Cu_2(\mu\text{-}OOCCH_3)_4{\cdot}2H_2O$ has been studied experimentally at 100 K and by DFT calculations on the isolated molecule using the Quantum Theory of Atoms In Molecules (QTAIMs). The bimetallic moiety is bridged by four equivalent acetate groups each other perpendicular and forming penta-atomic rings. The QTAIM parameters of charge density, its Laplacian, potential and kinetic energy density, delocalization indexes, static deformation density have been used to describe all intra- and intermolecular interactions. The topological analysis of the charge density maps shows the expected bond critical points with the corresponding bond paths, Cu–Cu bonding included. The data obtained using the different parameters and functions are consistent for all types of interatomic interactions, i.e. covalent, dative and intermetallic. The unpaired electrons responsible of the magnetic properties of d^9 Cu(II) ions occupy the orbitals pointing towards the acetate groups. The valence shell orbital populations of Cu(II) are consistent with the distortion of the octahedral coordination due to the Jahn–Teller effect.

1. Introduction

The transition metal–metal interaction in several bi- [1], tri- [2] and tetra-metallic complexes [3] has been the subject of several experimental and theoretical charge density studies [4]. In some of these compounds, the metal atoms are bridged by ligands and are part of triatomic rings. Only a few experimental charge density studies have been made on compounds where the metal–metal interaction is part of a wider ring, e.g. a penta-atomic ring. For example the $Cr_2(\mu\text{-}OOCCH_3)_4\_2H_2O$ compound has aroused inter-est owing to the abnormally short Cr–Cr bond and the topological properties of its charge density distribution have been studied using the deformation map approach [5]. A deep theoretical anal-ysis has been as well performed on dimers of $M_2(formamidinate)_4$ type with M = Nb, Mo, Tc, Ru and Pd [6,7], and on $Cu_2(\mu\text{-}OOCCH_3)_4\_2H_2O$ [8].

The opportunity to obtain accurate charge density maps, start-ing from low temperature X-ray diffraction data and using multi-polar refinement [9], has allowed to apply the Quantum Theory of Atoms In Molecules (QTAIM) [10] to a great number of com-pounds in order to derive topological properties [11]. The QTAIM correlates the bonding properties with the topology of the charge density, $\rho(r)$, and of its Laplacian, $\nabla^2\rho(r)$, obtainable by the sum of the three eigenvalues λ_1, λ_2 and λ_3 of the density Hessian matrix. The topological features of $\rho(r)$ and $\nabla^2\rho(r)$ are determined by their critical points (CPs), i.e. points where the first derivative of $\rho(r)$ vanishes. In a system in a stationary state and in a stable electro-static equilibrium (no net forces acting on the nuclei), interatomic interactions are defined by the presence of a bond path (a line of maximum density) and of a bond (3, -1) CP (BCP) along it. The inter-atomic bonds are classified on the basis of the sign and magnitude of $\nabla^2\rho(r)$ at the BCP ($\nabla^2\rho_{BCP}$). Closed-shell interactions are characterized by $\nabla^2\rho_{BCP} > 0$, that is by local depletion of charge density at the BCP, while shared-shell interactions have $\nabla^2\rho_{BCP} < 0$, that is local charge concentration at the BCP [10]. Further informa-tion can be obtained from the energy density values at BCPs, that is, the kinetic energy density, G_{BCP}, the potential energy density, V_{BCP}, and the total energy density, $H_{BCP} = G_{BCP} + V_{BCP}$, which can be estimated from the experimental density, its gradient and Laplacian [12].

Even if a bond path is not to be understood as representing a chemical bond in its more restricted meaning [13], the first papers, where QTAIM has been applied to X-ray experimental data of metal complexes, have invoked the presence of a bond path and of a (3, -1) BCP as a probe of the existence of a metal–metal link [1a,b,f,g,3b].

In spite of the small number of charge density studies of structures containing metal–metal bondings, in the past [2a] a tentative classification was made using the values of $\rho(r)$, $\nabla^2\rho(r)$, and the derived values of kinetic, potential and total en-ergy densities at BCP. These data were also compared with the

theoretical ones obtained for pure metals, in order to better understand the features of this non conventional bond [2a]. This attempt of classification was concluded with the statement that the intermetallic bond has 'its own topological features' [2a], and cannot be described by any pre-existent classification [1f,g]. In the meantime it has become clear that other properties and indi-cators must be taken into account to understand this 'atypical bond' [7], e.g. Delocalization Index values [14] and Source Func-tion analysis. In this paper, we report the results of a charge density study on hydrated copper acetate, $Cu_2(\mu\text{-}OOCCH_3)_4\_2H_2O$, the prototype of the wide family of dimeric copper(II) carboxyl-ates that in past have attracted considerable attention for their magnetic properties [15]. In the present context, hydrated cop-per acetate, a complex similar to the chromium acetate and to $M_2(formamidinate)_4$, represents a further example useful in the characterization of metal–metal bondings.

As it has been known since 1915, this compound has a much lower molar susceptibility at room temperature than usually ob-served for copper salts [16]. This abnormally low susceptibility was then confirmed by all subsequent investigations [17–21]. After some not conclusive discussions about the behavior of the suscep-tibility according to the Curie–Weiss law, the study of paramag-netic resonance absorption of powdered and single crystals samples of hydrated cupric acetate [22–25] allowed to suggest that the susceptibility curves could be explained by hypothesizing a crystalline structure where isolated pairs of copper atoms interact strongly through exchange forces. According to this, the abnor-mally low susceptibility has been attributed to the coupling be-tween unpaired electrons on adjacent copper atoms in singlet ground state and in the excited triplet state. The latter is responsi-ble for the paramagnetic properties observed at high temperatures. Later on it was determined that the single crystals reach a maxi-mum of susceptibility at nearly 255 K [26] and at 90 K a state of triplet is determined from the paramagnetic resonance spectrum [22].

Single crystal X-ray structure determinations [27,28] showed the dimeric structure of the compound with formula $Cu_2(\mu\text{-}CH_3COO)_4\_2H_2O$ [29], in which two copper atoms are bridged by four acetate groups and two water molecules occupy terminal positions on each Cu atom. The anomalous magnetic behavior of the cupric acetate was then ascribed to the dimeric structure of the compound, in which the copper–copper distance (2.64 Å) is only slightly greater than the same distance in metallic copper (2.56 Å), allowing a metal–metal interaction through exchange forces [30]. Theoretical models, based on both the MO and VB approaches, have led to the conclusion that any direct interaction is precluded between the two copper atoms [18–20,31–33]. A subsequent molecular orbital analysis [34,35] has concluded that "it is evident that the unpaired electron on each Cu occupies a $x^2\text{-}y^2$-like orbital oriented toward the four O atoms in the very nearly square-planar environment about the metal". Also estimations of exchange coupling constant, J, between copper atoms have been performed, using different theoretical approaches [36].

The focus of the present paper is the confirmation/rejection of the previous statements and in particular the existence of a copper–copper interaction and the comparison with data in other metal–metal bonds obtained in quite different complexes, for example complexes with neutral ligands (e.g. CO) instead of ionic ligands as acetate. For this purpose we have used low-temperature X-ray diffraction studies, combined with the results of quantum-chemical calculations. The experimental and theoretical electron density maps thus obtained have been analyzed within the QTAIM [10]. The Delocalisation Indexes for the interatomic interactions, the atomic charges, the d-orbitals population of Cu(II) ion and the static deformation density around Cu(II) are reported.

2. Experimental

2.1. Data collection

Blue-green prismatic crystals of copper acetate monohydrated (Fluka) have been crystallized from water solution and two crystals of different dimensions suitable for X-ray diffraction were selected. Both data sets have been collected at 100 K, with graphite-mono-chromatized Mo Ka radiation (λ = 0.71073 Å), with ω-scan method ($\Delta\omega$ = 1.0L) on an Gemini R Ultra diffractometer[1] equipped with low temperature device (N_2 stream).

Numerical absorption correction has been applied, separately on the two datasets, with faces accurately determined (μ = 3.17 mm^{-1}) and the data have been truncated at $\sin(\theta)/\lambda$ = 1.08 (θ_{max} = 50L). The two data sets have been then merged using XPREP [37] and the final number of independent reflections is 5251 (merged data R_{int} = 0.547). h, k, l limits: $-28 \le h \le 28$, $-18 \le k \le 18$, $-29 \le l \le 29$. Software used: CRYSALISPRO [38] (collec-tion, integration and absorption), SHELXTL [37] (structure solution, conventional refinement and molecular graphics).

Details about crystal data and data collection of the two data sets are reported in Table 1.

2.2. Multipolar refinement

Starting from the atomic parameters obtained from the conven-tional refinement, a multipole refinement has been performed according to the Hansen & Coppens formalism [39] as imple-mented in the XD2006 program suite [40].

Each pseudoatom has been assigned a core and spherical-va-lence scattering factor constructed from the STO atomic relativistic wavefunctions obtained at PBE/QZ4P level of theory for neutral atoms in the ground state configuration [41]. The single-ζ exponents have been obtained from Clementi and Roetti single-ζ functions [42]. Analytical spherical scattering factors are from International Tables for X-ray Crystallography [43].

The quantity minimized in the least-squares procedures was $\sum w(|F_o| - K|F_c|)^2$ and only the 4029 reflections with $F^2 > 3\sigma(F^2)$ and weights $w = 1/\sigma^2(F^2)$ were included in the multipolar refine-ment. The multipole expansion was truncated at the hexadecapole level for Cu, C and O atoms; for H atoms only one monopole and the dipoles in the bond direction have been refined. The valence densities of chemically equivalent atoms were constrained to be the same (the oxygen and carbon atoms of the acetate groups, the hydrogen atoms of the methyl groups and of the water mole-cule). For all atoms the neutral configuration has been used and electroneutrality constraints on the asymmetric unit have been ap-plied. The hydrogen atoms were refined riding to the bonded atom, with distances constrained to neutron values (1.09 Å for CH and 0.983 Å for OH) and $U(H) = 1.5 \_ U_{eq}(C)$ or $1.2 \_ U_{eq}(O)$.

The radial fit of the spherical valence density and of the defor-mation valence density have been optimized by refinement of their expansion–contraction parameters κ and κ' respectively. One j and one j^0 value has been refined for each Cu, O and C atom type. For the hydrogen atoms the values of j and j^0 have been fixed to the standard 1.2 value. Due to the great correlation of the expan-sion–contraction parameters with the thermal displacement parameters, the refinement has been performed in separate blocks. To test the effect of the anharmonicity in the thermal motion, third- and fourth-order Gram–Charlier coefficients have been introduced in the least squares procedures. Introduction of anhar-monic parameters led to no significant improvement in the multi-pole analyses, so they were excluded from the final model.

[1] Agilent Technologies UK Ltd., Oxford, UK.

Table 1
Some crystal data and collection parameters for the two data sets.

	Set I	Set II
Compound Formula M_r	$C_8 H_{16} Cu_2 O_{10}$ 399.29	$C_8 H_{16} Cu_2 O_{10}$ 399.29
Crystal system, space group	monoclinic, C2/c	monoclinic, C2/c
Unit cell parameters (Å, °)	a = 13.0834(1)	a = 13.0830(2)
	b = 8.5028(1)	b = 8.5017(1)
	c = 13.7315(1)	c = 13.7330(2)
	β = 116.865(1)	β = 116.857(2)
Unit cell volume ($Å^3$)	1362.70(1)	1362.73(1)
Z	4	4
ρ_{calc} (g cm^{-3})	1.946	1.946
F(000)	808.0	808.0
Radiation type	Mo Kα	Mo Kα
Data collection method	ω-scan	ω-scan
θ range (°)	3–67.07	3–67.10
Range of h, k, l	-33 < h < 33	-33 < h < 34
	-19 < k < 19	-21 < k < 21
	-31 < l < 35	-35 < l < 36
Temperature (K)	100(2)	100(2)
Crystal size (mm)	0.1081 x 0.0954 x 0.0701	0.1595 x 0.1076 x 0.0511
Absorption correction	Gaussian	Gaussian
T_{min}, T_{max}	0.789, 0.846	0.711,0.888
No. of measured, independent and observed reflections	105180, 5169, 4287	33122, 3415, 2970
Criterion for observed reflection	$F_o > 4\sigma(F_o)$	$F_o > 4\sigma(F_o)$
R_{int} [a], R_σ [b]	0.0472, 0.0456	0.0575, 0.666
Multipolar refinement results on merged data		
Refinement on	F^2	
No. of reflections	5251	
No. of parameters	225	
H-atom treatment	Mixed of independent and constrained refinement	
Weighting scheme	$w = 1/\sigma^2(F_o^2)$	
$R(F^2)$, $wR(F^2)$, S	0.0197, 0.0173, 1.147	
Shift/e.s.d.	<0.001	
$\Delta\rho_{max}$, $\Delta\rho_{min}$ (e $Å^{-3}$)	0.40, -0.41	

[a] $R_{int} = [\Sigma(|F_o^2 - F_o^2(mean)|)/\Sigma F_o^2$.

[b] $R_\sigma = [\Sigma(\sigma(F_o^2)]/\Sigma F_o^2$.

The Hirshfeld [44] rigid-bond criterion is fulfilled by the C–C and C–O bonds (mean Δ-msda = 0.6 _ 10^{-3}), instead the Cu–O bonds slightly exceed the criterion (mean Δ-msda = 1.8 _ 10^{-3}).

All parameters of the final multipole model are collected in the CIF file of the Supplementary material.

2.3. Computational details

Calculations have been carried out at the ROB3LYP/6-311++G✓ level of theory on the dimeric structure of monohydrated copper acetate, $Cu_2(CH_3COO)_4$_$2H_2O$, in the gas phase, using the GAUSSIAN 09 code [45]. Topological analysis of electron density distribution by QTAIM has been performed with the AIMPAC program [46].

Calculations have been performed on the experimental geometry at 100 K at the triplet state (state determined from the para-magnetic resonance spectrum at that temperature) [22]. The use of the experimental, fixed geometry instead of the optimized, equilibrium one, was dictated by the fact that geometry optimization of the complex in the gas phase, at the same level of theory, led to non negligible discrepancies with the experimental geometry in the Cu(1)–O(3) (Δ = 0.065 Å), Cu(1)–O(4) (Δ= 0.047 Å) and Cu(1)– O(5) (Δ = 0.162 Å) distances. Such discrepancies are to be clearly ascribed to strong intermolecular interactions detected in the crystal structure, involving atoms O(3), O(4) and O(5) (see Section 3). The use of the experimental geometry allowed to recover a good agreement of the computed BCP topological properties with the experimental ones also for that bonds connecting atoms which are involved in strong intermolecular interactions, making reliable the results obtained with calculations on the isolated molecule. It is also to be pointed out that, on the other hand, the optimized RO-B3LYP/6-311++G✓ intramolecular Cu–Cu distance, 2.5983 Å, well reproduced the experimental value, 2.6107(4) Å, suggesting no significant influence of the crystal environment on the metal–metal interaction, which is the main focus of the present work.

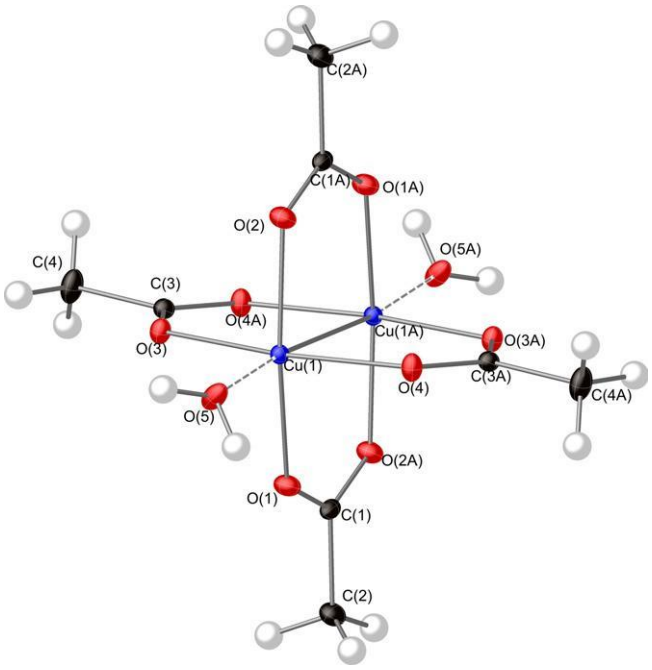

Fig. 1. ORTEP plot of $Cu_2(CH_3COO)_4 \cdot 2H_2O$ with thermal parameters at 50% of probability. Atoms with label A are related to the corresponding ones by the crystallographic inversion centre.

Table 2
Critical points properties from multipolar analysis at 100 K (first line) and from DFT/B3LYP single point calculations on the experimental geometry (second line).

	Bond length (Å)	ρ_{BCP} (e Å^{-3})	$\nabla^2\rho_{BCP}$ (e Å^{-5})	G_{BCP} (hartree Å^{-3})	V_{BCP} (hartree Å^{-3})	H_{BCP} (hartree Å^{-3})	$\lvert\lambda_1\rvert/\lambda_3$
Bond critical points							
Cu(1)–Cu(1A)	2.6107(4)	0.182(1)	1.68(1)	0.12	_0.13	_0.01	0.16
		0.199	1.58	0.16	_0.21	_0.05	0.22
Cu(1)–O(1)	1.9831(5)	0.512(4)	9.06(1)	0.69	_0.74	_0.05	0.17
		0.548	10.92	0.82	_0.87	_0.05	0.17
Cu(1)–O(2)	1.9900(6)	0.521(1)	9.22(1)	0.70	_0.76	_0.06	0.18
		0.535	10.62	0.79	_0.84	_0.05	0.16
Cu(1)–O(3)	1.9536(6)	0.558(1)	9.86(1)	0.76	_0.84	_0.08	0.18
		0.584	12.06	0.90	_0.96	_0.06	0.16
Cu(1)–O(4)	1.9411(6)	0.595(1)	10.47(1)	0.83	_0.92	_0.09	0.18
		0.604	12.64	0.95	_1.01	_0.06	0.17
Cu(1)–O(5)	2.1474(9)	0.378(6)	6.07(1)	0.44	_0.46	_0.02	0.19
		0.349	6.08	0.46	_0.49	_0.03	0.17
O(1)–C(1)	1.2681(8)	2.55(3)	_27.6(2)	2.5	_7.0	_4.7	1.44
		2.45	_9.9	3.2	_7.1	_3.9	0.67
O(2)–C(1)	1.2685(8)	2.62(3)	_28.8(1)	2.7	_7.3	_4.6	1.42
		2.44	_9.9	3.2	_7.1	_3.9	0.67
O(3)–C(3)	1.2733(9)	2.54(1)	_27.3(1)	2.5	_6.9	_4.4	1.40
		2.42	_10.4	3.1	_6.9	_3.8	0.68
O(4)–C(3)	1.2607(9)	2.74(1)	_34.6(1)	1.4	_3.6	_2.2	1.64
		2.48	_8.9	3.4	_7.3	_4.0	0.64
C(1)–C(2)	1.5057(9)	1.81(2)	_13.5(7)	1.5	_4.0	_2.5	1.08
		1.75	_15.5	0.4	_1.9	_1.5	1.42
C(3)–C(4)	1.506(1)	1.69(1)	_10.7(1)	1.4	_3.6	_2.2	0.99
		1.75	_15.6	0.4	_1.9	_1.5	1.42
C(2)–H(2A)	1.09	1.64(3)	_11.84(8)	1.3	_3.4	_2.1	0.87
		1.85	_22.0	0.3	_2.1	_1.8	1.42
C(2)–H(2B)	1.09	1.51(2)	_10.18(7)	1.1	_3.0	_1.9	0.88
		1.85	_21.9	0.3	_2.1	_1.8	1.42
C(2)–H(2C)	1.09	1.66(2)	_13.66(7)	1.2	_3.4	_2.2	0.95
		1.87	_22.5	0.3	_2.1	_1.8	1.41
C(4)–H(4A)	1.09	1.66(1)	_13.66(1)	1.2	_3.4	_2.2	0.95
		1.87	_22.4	0.3	_2.1	_1.8	1.41
C(4)–H(4B)	1.09	1.64(1)	_11.84(1)	1.3	_3.4	_2.1	0.87
		1.85	_22.1	0.3	_2.1	_1.8	1.42
C(4)–H(4C)	1.09	1.63(1)	_13.38(1)	1.2	_3.3	_2.1	0.93
		1.84	_21.8	0.3	_2.1	_1.8	1.41
O(5)–H(5A)	0.983	2.13(3)	_27.5(2)	1.6	_5.0	_3.4	0.91
		2.31	_55.0	0.4	_4.7	_4.3	1.74
O(5)–H(5B)	0.983	2.15(2)	_28.7(7)	1.5	_5.1	_3.6	0.93
		2.32	_55.0	0.4	_4.8	_4.3	1.75
Ring critical points							
Cu(1)–O(1)–C(1)–O(2)–Cu(1A)			0.119(1)	1.1(1)			
			0.104	1.2			
Cu(1)–O(3)–C(3)–O(4)–Cu(1A)			0.124(1)	1.1(1)			
			0.107	1.3			

3. Results and discussion

3.1. Molecular structure

The $Cu_2(\mu\text{-}OOCCH_3)_4{\cdot}2H_2O$ salt can be considered as a coordination compound and its molecule lies on a crystallographic inver-sion centre and is formed by two Cu(II) atoms bridged by four acetate moieties; each Cu atom links also to a water molecule (Fig. 1). The coordination around Cu atoms forms a distorted octa-hedral geometry due to the well-known Jahn–Teller effect for d^9 transition metals.

3.2. Topological analysis of experimental and theoretical charge density distribution

In Table 2 the (3, -1) BCP and (3,+1) ring critical points (RCP) of charge density are listed, as obtained from experiment and from ROB3LYP/6-311++G** single point calculations on the experimental geometry at 100 K, together with the energy density values at the BCPs. In particular, the experimental G_{BCP} values are estimated through an approximate formula from the experimental Laplacian [12] and the V_{BCP} values are calculated from the Local Virial Theorem using the approximated G_{BCP}. Such estimated energy densities are known to be more reliable for closed-shell interactions ($\nabla^2\rho_{BCP} > 0$) than for shared interactions ($\nabla^2\rho_{BCP} < 0$).

A good agreement is observed between the results of the two analyses, with the only expected exception of the $\nabla^2\rho_{BCP}$ values of the CO bonds, owing to the well known fact that, for polar bonds, the BCP is usually placed in a region where the parallel curvature (λ_3) changes considerably, making plausible even large differences between experimental and theoretical Laplacian values [47]. All BCPs are characterized by ρ_{BCP} and $\nabla^2\rho_{BCP}$ values in keeping with shared (C–O and C–H bonds) and closed shell (Cu–O and Cu–Cu bonds) behavior, according to the classical classification of QTAIM [10] (Fig. 2).

Both experimental and theoretical analyses agree about the presence of a Cu–Cu bond path (see Table 2 and Fig. 2a), whose features at the BCP are similar to those observed in other metal–metal bonding found in metal complexes [1–3]: low charge density, po-sitive Laplacian, H_{BCP} negative and close to zero, and ratio |V|/G be-tween 1 and 2 (1.1 from experiment and 1.3 from theory).

Fig. 2b shows the flatness of the zone corresponding to the metal–metal interaction, characterized by a low population in

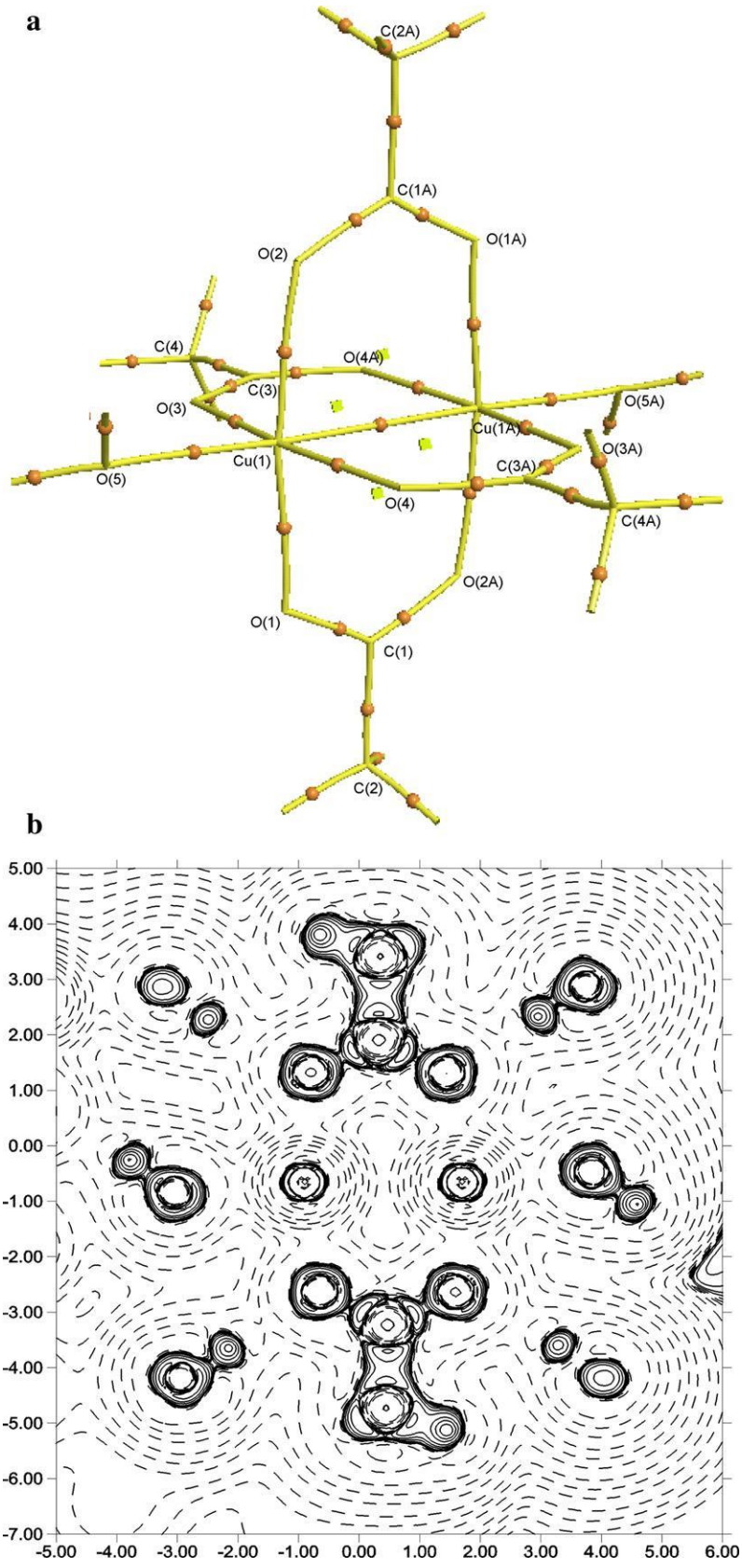

Fig. 2. (a) Molecular graph of copper acetate monohydrate with BCPs (yellow spheres) and RCPs (green cubes) superimposed. Only atoms in the asymmetric unit are labeled. (b) Experimental Laplacian $-\nabla^2\rho(r)$ maps in the Cu(1)Cu(1a)O(1)O(2a) plane. The absolute value of the contours (a.u.) increases from the outermost inwards in steps of 2×10^n, 4×10^n, 8×10^n, n beginning at -3 and increasing in steps of one. Positive values of $-\nabla^2\rho(r)$ are denoted by dashed contours, negative values by solid contours. Only atoms of the asymmetric unit are labeled. (For interpretation of the references to colour in this figure legend, the reader is referred to the web version of this article.)

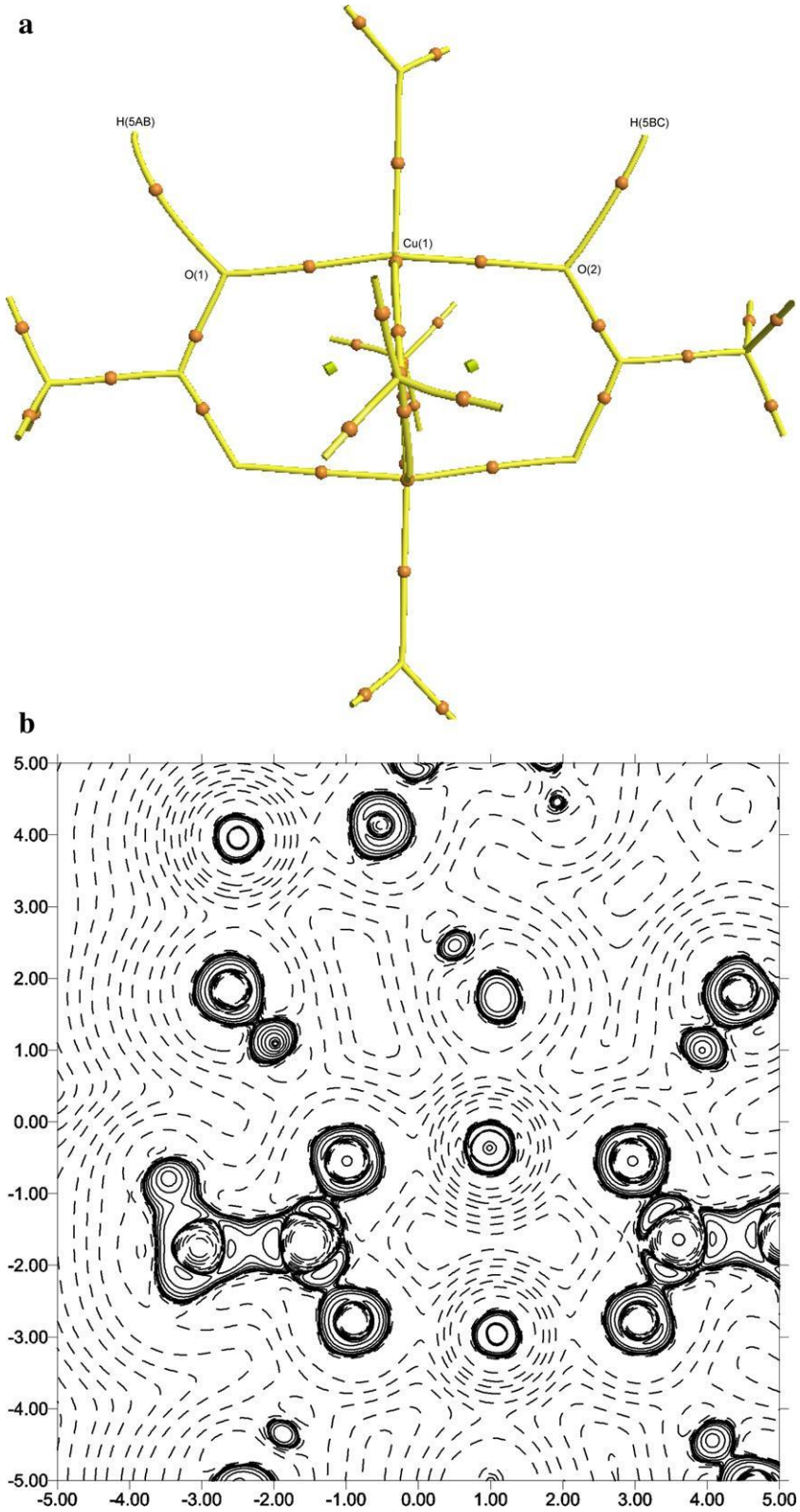

Fig. 3. (a) Molecular graph of copper acetate monohydrate with BCPs (yellow spheres) and RCPs (green cubes) superimposed. Only atoms involved in hydrogen bonds are labeled. (b) Laplacian of $\rho(r)$ in the H(5AB)–O(1)–Cu(1)–O(2)–H(5BC) plane. The absolute value of the contour (a.u.) increases from the outermost inwards in steps of 2 x 10^n, 4 x 10^n, 8 x 10^n, n beginning at -3 and increasing in steps of one. Positive values of $-\nabla^2\rho(r)$ are denoted by dashed contours, negative values are denoted by solid contours. Only atoms involved in hydrogen bonds are labeled. (For interpretation of the references to colour in this figure legend, the reader is referred to the web version of this article.)

the valence basin, as observed in other binuclear complexes with metal–metal bonding [11,48]. Also the ratio of the principal curvatures $|\lambda_1|/\lambda_3$, reported in Table 1, provides information for a classification of chemical bonding [49]. A curvature ratio $<<1$ is typical

Table 3

Geometrical and topological parameters of the stronger hydrogen bonds in hydrated cupric acetate (atoms H(5AB) and H(5BC) correspond to the water molecules symmetry related: 1-x, 2.5-y, 1-z, and -x, y, 0.5-z, respectively).

	Bond length (Å)	Bond path length (Å)	Angle A···H–D (°)	Distance A···D (Å)	ρ(e Å^{-3})	$\nabla^2\rho$ (e Å^{-5})
O(1)···H(5AB)	1.9128	1.9840	168.41	2.883	0.08(1)	2.568(9)
O(2)···H(5BC)	1.7991	1.8066	178.54	2.782	0.11(1)	3.972(1)

Table 4

X-ray derived, q_{exp}, and theoretical, q_{theo}, integrated net charges of hydrated cupric acetate as obtained by QTAIM partitioning.

	q_{exp} (e)	q_{theo} (e)
Cu(1)	0.41	1.20
O(1)	-0.99	-1.14
O(2)	0.91	-1.16
O(3)	-0.98	-1.15
O(4)	-0.95	-1.14
O(5)	-1.17	-0.91
C(1)	1.29	1.55
C(2)	-0.36	0.03
C(3)	1.31	1.56
C(4)	-0.35	0.03
H(2A)	0.26	0.03
H(2B)	0.23	0.03
H(2C)	0.23	0.03
H(4A)	0.23	0.03
H(4B)	0.26	0.03
H(4C)	0.22	0.03
H(5A)	0.63	0.48
H(5B)	0.62	0.48
Acetate C(1)C(2)O(1)O(2)group	-0.25	-0.72
Acetate C(3)C(4)O(3)O(4)group	-0.26	-0.70
Water molecule O(5)H(5A)H(5B)	0.08	0.05

Table 5

Experimental and ROB3LYP/6-311++G** theoretical copper atomic d-orbital populations (%).

	d_z^2	dxz	dyz	dx^2-y^2	dxy
Experiment	21.4	20.4	21.2	15.5	21.4
Theory	21.2	21.5	21.5	14.6	21.1

for closed-shell interactions, such as Cu–Cu and Cu–O in copper acetate, while a $|\lambda_1|/\lambda_3 \geq 1$ has been found for shared interactions. For the latter this value increases with bond strength: in fact the ratio for C–O acetate bonds, almost double bonds, is greater than for C–H bonds.

The presence of the Cu–Cu bond path in hydrated cupric acetate is unexpected, considering that the Cu–Cu bond is bridged by even four ligands. There are in fact some cases where no intermetallic bond path was detected, though only one atom bridges the metal-metal bond forming a triatomic ring [1c,d,2c,11b].

About the other interactions, in the hydrated cupric acetate there are three types of Cu–O bonds, two involving the acetate oxygen atoms, Cu(1)–O(3,4) and Cu(1)–O(1,2), and one involving the water oxygen atoms Cu(1)–Ow(5). The four equatorial Cu(1)–O(1,2,3,4) bonds show similar ρ_{BCP} (0.51–0.59 e Å_3), while the longer Cu(1)–Ow(5) has a lower ρ_{BCP} (0.38 e Å^{-3}). The Cu(1)–O(1,2) bond distances are longer than the Cu(1)–O(3,4) bond lengths, because O(1) and O(2) atoms are involved in hydrogen bonds with water molecules of symmetry related molecules (see Fig. 3 and Table 3). The values of ρ_{BCP} correlate with the Cu–O distances also in this basal plane. The slightly negative H_{BCP} all Cu–O interactions can correspond to a very small covalent character in addition to the main ionic features. In spite of the small negative H_{BCP}, the Cu–O interactions, with positive Laplacian, $|V|/G > 1$, and $|k_1|/k_3$ _ 1, belong clearly to the transit closed shell type [1i].

The Cu(1)–O(1)–O(2)–O_W(5C)–H(5CB) and O_W(5B)–H(5BA) atoms lie in a plane with a mean deviation of 0.0428 Å. The bond paths and the corresponding BCPs associated to these hydrogen bonds and the Laplacian map are shown in Fig. 3 and in Table 3 the geometrical properties and the topological parameters are reported. According to a hydrogen bond classification based on geometrical parameters[50] (D–H···A angle, D···A and H···A distances) their features correspond to strong hydrogen bonds, in agreement with the relatively high ρBCP (0.11–0.15 e Å^{-3}). Other (3, -1) CPs associated to O···H interactions have been found, they have however low ρ_{BCP} and therefore they have been omitted from Table 3.

3.3. Atomic charges

QTAIM theory affords also criteria for a partitioning of molecular systems into atomic subsystems, constituted by the combination of a nuclear attractor (nucleus) and a corresponding atomic basin, Ω: the latter is defined by interatomic surfaces that satisfy the zero flux condition of the gradient vector field of charge density. The integration of $\rho(r)$ over the atomic basins gives the atomic charges: $q(\Omega) = Z$ -$N(\Omega)$, where Z is the atomic number and $N(\Omega) = \int_\Omega \rho(r)dr$. The atomic charges for the investigated structure, as obtained by QTAIM partitioning of both experimental and computed charge density distributions, are reported in Table 4. In both cases, the values obtained for the copper atom and the acetate ions were lower than the formal charges of $Cu^{2+}(CH_3COO^-)_2$, though a significant charge transfer occurs in the correct direction from acetate moieties to copper ions. On the other hand, as expected, water molecule remains almost neutral, underlining the weakness of the Cu–Ow interaction with respect the Cu–Oac ones. By looking at the individual values of atomic charges, experiment and theory in general do not agree very well. Quite similar discrepancies were however observed by Farrugia et al. in their charge density study of 3-amino-propanolato Cu(II) binuclear complexes [51]; these discrepancies were ascribed to some degree of ambiguity in the experimental charges of transition metals.

3.4. d-Orbital populations

d-Orbital populations have been obtained from X-ray data through the method of Coppens et al. [52] They are listed in Table 5 together with the theoretical values, as obtained from NBO analysis [53] on the ROB3LYP/6-311++G** wavefunction. Interestingly, experimental and theoretical values, obtained through completely different approaches, show the same trend. The x and y directions point towards the acetate ligands, while the elongated Cu(1)–Cu(1A) and Cu(1)–O(5) bonds lie along the z direction. In a regular elongated octahedral environment the percentage of population must be 11.1% in the $d_{x^2-y^2}$ and 22.2% in the other four d orbitals. In copper acetate the populations agree well with the expected splitting of the orbitals for a d^9 configuration and show that only the $d_{x^2-y^2}$ orbital, towards the acetate ligands, is not fully occupied due to the strong Jahn–Teller effect and therefore corresponds to the magnetic orbital [8]. The high population of $d_{x^2-y^2}$ with respect to a regular distorted octahedron is also the result of the σ and π donation toward and from Cu atom, according to the Dewar–Chatt–Duncanson metal–ligand model. Owing tothe charges

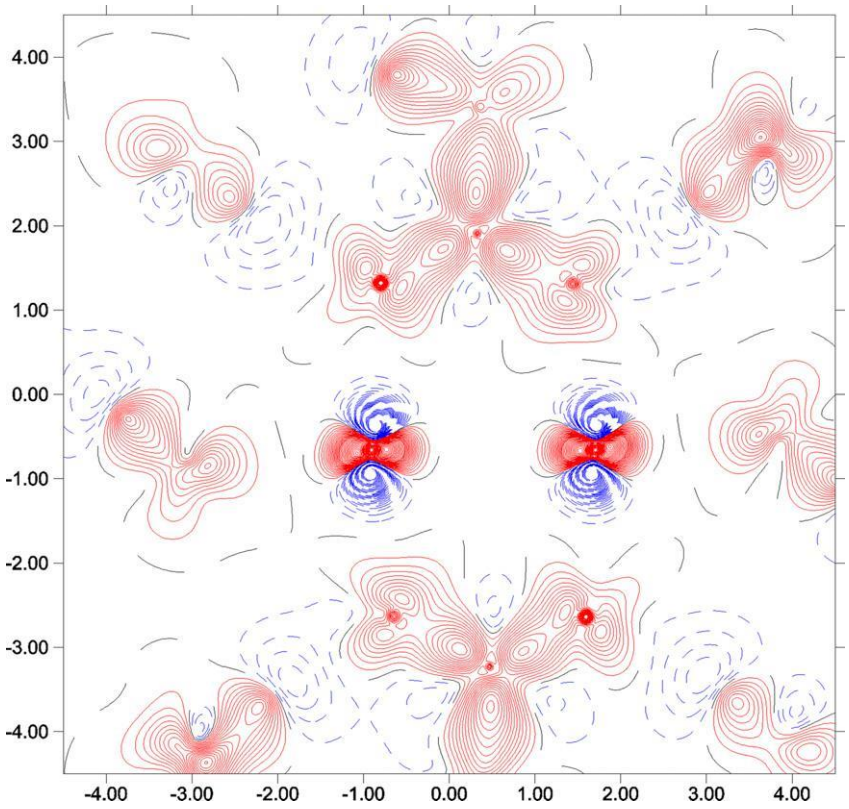

Fig. 4. Deformation density map in Cu(1)–O(1)–C(1) plane. Contours are at 0.1 e $Å^{-3}$. Blue broken lines are negative value, red positive and black is 0 value. (For interpretation of the references to colour in this figure legend, the reader is referred to the web version of this article.)

reported above it can be concluded that the r donation is greater than the π Cu withdrawing.

3.5. Electron deformation density

Fig. 4 shows the static deformation density defined as the difference between the model ($\rho_{mult}(r)$, from multipole model) and a reference ($\rho_{IAM}(r)$, from the Independent Atom Model, IAM) elec-tron densities: $\Delta q = \rho_{mult}-\rho_{IAM}$. Fig. 4 clearly shows the charge distribution in the plane containing the Cu atoms and two acetate bridges.

The acetate O atoms O(1) and O(2) exhibit positive deformation densities directed toward the Cu atom, owing to the polarization of the O valence electron shell under the Cu–O coordination interac-tions. Such deformation is related to a formal sp^2 configuration of oxygen atoms. The same behavior is shown by O(3), O(4) in the plane containing the perpendicular acetate. Correspondingly, a large electron density depletion in the copper electron valence shell (VS) shows up in the Cu–O(1,2,3,4) directions. Maxima of the VS can be evidenced by$_0$ (3, -3) critical points of $\nabla^2\rho(r)$; they are at a distance of 0.28 ÅA av. as in other similar compounds [51,54] and disposed among the ligands, while charge depletions, (3,+1) CPs $\nabla^2\rho(r)$, are located along the direction of the four ace-tate oxygen atoms at the same distance. The absence of a charge depletion in Cu valence shell in the direction of the weaker Cu– Cu and Cu–Ow interactions is due to the great deformation of the O_h versus a tetragonal bipyramidal geometry.

3.6. Delocalization index

Another instrument useful to characterize chemical bonding in molecules is the delocalization index, $\delta(A,B) = 4\int\Omega(A)dr1\int_{\Omega(B)}dr_2\rho(r_1,r_2)$-2N(A)N(B), where $\rho(r_1,r_2)$ is the two-particle density for electrons of parallel spin [55]. δ(A,B) provides a quantitative measure of the sharing or the exchanging of electrons be-tween two atoms A and B, and can be interpreted as a measure of the extent to which the electrons in A are delocalized onto atom B and vice versa. δ(A,B) is not restricted to atoms sharing a com-mon interatomic surface, so that it may be computed for any pair of atoms; therefore it is an indicator able to depict the ‘‘electronic communication’’ between atoms, regardless of whether there is or not a formal bond between them [11b]. It cannot be related to bond order, but at the Hartree–Fock level, and for equally shared electron pairs, δ(A,B) is simply the number of pairs of shared elec-trons. In Table 6 the delocalization indexes computed on the RO-B3LYP/6-311++G″ wavefunction for all inter-atomic interactions found in the title compound are reported. For all C–C and C–H bonds of acetate moieties we have found δ(C,C) and δ(C,H) close to one, as typical for such covalent single bonds; on the other hand, for all C-O and O-H bonds the delocalization indices were smaller than those predicted by their bond order, indicating a lower shar-ing of electrons for such polar bonds. The delocalization indexes

Table 6
Delocalization Indexes (A,B) for copper acetate mono-hydrate, calculated at ROB3LYP/6-311++G″ level of theory.

Atom pairs, A-B	δ(A,B)
Cu-Cu	0.129
(Cu-Oac)av	0.373
Cu-Ow	0.248
(C-O)av	1.089
(C-C)av	0.928
(C-H)av	0.953
(O-H)av	0.675

obtained for metal–ligand bonds are quite typical for these kinds of interactions [3a,4,2c,11b,51], with average values δ(Cu,Oac) = 0.373 and δ(Cu,Ow) = 0.248, significantly lower than those of the strong covalent C-C and C-O bonds. The value of the delocalization index found for Cu–Cu bonding (δ(Cu,Cu) = 0.129) is significant, also compared with the value found in other similar compounds in which no bond path has been found between copper atoms (see Ref. [51]). This small value obtained for the Cu–Cu bond in copper acetate, if compared with those of the other types of bonds (Cu–O, C–C, C–O, C–H), should indicate a rather small electron delocalization in the internuclear metallic region (high Pauli repulsion).

4. Conclusions

We have reported the charge distribution of the antiferromag-netic copper acetate $Cu_2(\mu\text{-}OOCCH_3)_4{\cdot}2H_2O$ obtained from high resolution single crystal X-ray diffraction data using a multipolar refinement of experimental data and from theoretical calculations. We have analysed the intra- and inter-molecular interactions using different parameters, e.g. the delocalisation indexes for the inter-atomic interactions and the static deformation density around Cu(II). The atomic charges of all atoms and the orbital populations of Cu(II) ion have been obtained. Our interest has been focused mainly on the characterization of the Cu–O and Cu–Cu interac-tions. The Cu–O interaction is mainly driven by ionic contributions and a prevailing r charge transfer from acetate to Cu atom can be deduced. The calculated d-orbital populations agree with the pres-ence of the unpaired electron on copper $d_{x^2-y^2}$ atomic orbital: from this result, as already pointed out by other authors for similar com-pounds [51,54], it can be stated that this represents the magnetic orbital, the favorite way through which the superexchange interac-tion between copper ions occurs.

A bond path and a suitable delocalization index value confirm the presence of a direct Cu–Cu interaction, with features in agree-ment with other intermetallic bondings of transition elements in complexes and in bulk metals [1,2]. In these interactions the ki-netic and potential energy density nearly compensate each other, leading to a negligible total energy density value. This is the first compound where a metal–metal moiety bridged by four ligands shows the topological features of a real interaction between met-als, supported by a bond path and by a BCP and not only by a bond distance value.

The coordination around the Cu atoms is strongly distorted from an octahedral geometry to a square planar bipyramid. This behavior is depicted by the Laplacian and by the static deformation maps; it can be stressed that all experimental and theoretical data supply the same description of chemical bondings in the title compound.

Acknowledgments

Research financially supported by MIUR [Roma, PRIN 2007 pro-ject "Compositional and structural complexity in minerals (crystal chemistry, microstructures, modularity, modulations): analysis and applications"]. A.F. acknowledges CASPUR for computational resources within the project "Standard HPC Grant 2010".

Appendix A. Supplementary data

CCDC 812312 contains the supplementary crystallographic data for $Cu_2(\mu\text{-}OOCCH_3)_4{\cdot}2H_2O$. These data can be obtained free of charge via http://www.ccdc.cam.ac.uk/conts/retrieving.html, or from the Cambridge Crystallographic Data Centre, 12 Union Road, Cambridge CB2 1EZ, UK; fax: (+44) 1223-336-033; or e-mail: deposit@ccdc.cam.ac.uk.

References

[1] (a) R. Bianchi, G. Gervasio, D. Marabello, Chem Commun. 15 (1998) 1535;
(b) R. Bianchi, G. Gervasio, D. Marabello, Inorg. Chem. 39 (2000) 2360;
(c) R. Bianchi, G. Gervasio, D. Marabello, D. Helvetica, Chim. Acta 84 (2001) 722;
(d) R. Bianchi, G. Gervasio, D. Marabello, Acta Crystallogr., Sect. B 57 (2001) 638;
(e) R. Bianchi, G. Gervasio, D. Marabello, C. R. Chim. 8 (2005) 1392;
(f) L.J. Farrugia, P.R. Mallinson, B. Stewart, Acta Crystallogr., Sect. B 59 (2003) 234;
(g) P. Macchi, D.M. Proserpio, A. Sironi, J. Am. Chem. Soc. 120 (1998) 13429;
(h) G. Jansen, M. Schubart, B. Findeis, L.H. Gade, I.J. Scowen, M.J. McPartlin, Am. Chem. Soc. 120 (1998) 7239;
(i) G. Gervasio, R. Bianchi, D. Marabello, Chem. Phys. Lett. 387 (2004) 481.
[2] (a) G. Gervasio, R. Bianchi, D. Marabello, Chem. Phys. Lett. 407 (2005) 18;
(b) G. Gervasio, D. Marabello, R. Bianchi, A. Forni, J. Phys. Chem. A 114 (2010) 9368;
(c) L.J. Farrugia, C. Evans, C.R. Chimie, C. R. Chim. 8 (2005) 1566.
[3] (a) P. Macchi, L. Garlaschelli, S. Martinengo, A. Sironi, J. Am. Chem. Soc. 121 (1999) 10428;
(b) W. Uhl, S. Melle, G. Frenking, M. Hartmann, Inorg. Chem. 40 (2001) 750.
[4] L.J. Farrugia, H.M. Senn, J. Phys. Chem. A 114 (2010) 13418.
[5] M. Bernard, P. Coppens, M.L. DeLucia, E.D. Stevens, Inorg. Chem. 19 (1980) 1924.
[6] R. Llusar, A. Beltran, J. Andrès, F. Fuster, B. Silvi, J. Phys. Chem. A 105 (2001) 9460.
[7] C. Gatti, D. Lasi, Faraday Discuss. 135 (2007) 55.
[8] P.J. Hay, J.C. Thibeault, R. Hoffmann, J. Am. Chem. Soc. 97 (1975) 4884.
[9] R.F. Stewart, Acta Crystallogr., Sect. A 32 (1976) 565.
[10] R.F.W. Bader, Atoms in Molecules – A Quantum Theory, Oxford University Press, Oxford, 1990.
[11] (a) T.S. Koritsanszky, P. Coppens, Chem. Rev. 101 (2001) 1583;
(b) P. Macchi, A. Sironi, Coord. Chem. Rev. 238–239 (2003) 383.
[12] (a) D.A. Kirzhnits, Sov. Phys. JETP 5 (1957) 64;
(b) Yu.A. Abramov, Acta Crystallogr., Sect. A 53 (1997) 264;
(c) E. Espinosa, E. Molins, C. Lecomte, Chem. Phys. Lett. 285 (1998) 170.
[13] R.F.W. Bader, J. Phys. Chem. A 113 (2009) 10391.
[14] L.J. Farrugia, C.S. Frampton, J.A.K. Howard, P.R. Mallinson, R.D. Peacock, G.T. Smith, B. Stewart, Acta Crystallogr., Sect. B 62 (2006) 236.
[15] M. Kato, H.B. Jonassen, J.C. Fanning, Chem. Rev. 64 (1964) 99.
[16] V.J. Lifschitz, E.Z. Rosenbohm, Elektrochemie (1915) 499.
[17] M.J. Amiel, Compt. Rend. 207 (1938) 1097.
[18] A. Mookerjee, Indian J. Phys. 19 (1945) 63.
[19] B.C. Guha, Proc. R. Soc. A 206 (1951) 353.
[20] G. Foex, T. Karantassis, N. Perakis, Compt. Rend. 237 (1953) 982.
[21] M.J. Gauthier, Compt. Rend. 238 (1954) 1999.
[22] B. Bleaney, K.D. Bowers, Proc. R. Soc. A 214 (1952) 451.
[23] B. Bleaney, K.D. Bowers, Philos. Mag. 43 (1952) 372.
[24] H. Kumagai, H. Abe, H.J.A. Shimada, Phys. Rev. 87 (1952) 385.
[25] H.J.A. Shimada, Phys. Rev. 90 (1953) 316.
[26] A. Mookherji, S.C. Mathur, J. Phys. Soc. Jpn. 18 (1963) 977.
[27] J.N. Van Niekerk, F.R.L. Schoening, Acta Crystallogr. 6 (1953) 227.
[28] P. De Meester, S.R. Fletcher, A.C. Skapski, J. Chem. Soc., Dalton Trans. (1973) 2575.
[29] This compound has been found in Potosi open pit, Broken Hill, New South Wales (Australia) by Graham P. Hogan (1957), with small impurities of Fe(II), and it is known as mineral hoganite. D.E. Hibbs, U. Kolitsch, P. Leverett, J.L. Sharpe, P.A. Williams, Mineral. Mag. 66 (2002) 459.
[30] (a) B.N. Figgis, R.L. Martin, J. Chem. Soc. (1956) 3837;
(b) A.W. Schlenter, R.A. Jacobsen, R.E. Rundle, Inorg. Chem. 5 (1966) 277;
(c) A.E. Hansen, C.J. Ballhausen, Trans. Faraday Soc. 61 (1965) 631;
(d) G.F. Kokoszka, M. Linzer, G. Gordon, Inorg. Chem. 7 (1968) 1730;
(e) R.W. Jotham, S.F.A. Kettle, Inorg. Chem. 9 (1970) 1390.
[31] I.G. Ross, Trans. Faraday Soc. 55 (1959) 105.
[32] I.G. Ross, J. Yates, Trans. Faraday Soc. 55 (1959) 1064.
[33] M.L. Tonnet, S. Yamada, I.G. Ross, Trans. Faraday Soc. 60 (1964) 840.
[34] G.F. Kokoska, H.C. Allen, G. Gordon, J. Chem. Phys. 42 (1965) 3693.
[35] P.J. Hay, J.C. Thibeault, R. Hoffmann, J. Am. Chem. Soc. 97 (1975) 4884.
[36] E. Ruiz, M. Llunell, P. Alemany, J. Solid State Chem. 176 (2003) 400.
[37] G.M. Sheldrick, SHELXTL, Göttingen, Germany, 1997.
[38] Agilent Technologies, CrysAlisPro Software System, Version 1.171.35.19, Agilent Technologies UK Ltd., Oxford, UK, 2012.
[39] N.K. Hansen, P. Coppens, Acta Crystallogr., Sect. A 34 (1978) 909.
[40] A. Volkov, P. Macchi, L.J. Farrugia, C. Gatti, P.R. Mallinson, T. Richter, T. Koritsanszky, XD2006 – a computer program for multipole refinement, topological analysis and evaluation of intermolecular energies from experimental and theoretical structure factors, 2006. Available from: <http:// xd.chem.buffalo.edu/>.
[41] A. Volkov, P. Macchi, unpublished work.
[42] E. Clementi, C. Roetti, At. Data Nucl. Data Tables 14 (1974) 177.

[43] C.K. Johnson, H.A. Levy, International Tables of X-Ray Crystallography, vol. IV, Kynoch Press, Birmingham, 1974.
[44] F.L. Hirshfeld, Acta Crystallogr., Sect. A 32 (1976) 239.
[45] M.J. Frisch, G.W. Trucks, H.B. Schlegel, G.E. Scuseria, M.A. Robb, J.R. Cheeseman, G. Scalmani, V. Barone, B. Mennucci, G.A. Petersson, H. Nakatsuji, M. Caricato, X. Li Hratchian, A.F. Izmaylov, J. Bloino, G. Zheng, J.L. Sonnenberg, M. Hada, M. Ehara, K. Toyota, R. Fukuda, J. Hasegawa, M. Ishida, T. Nakajima, Y. Honda, O. Kitao, H. Nakai, T. Vreven, J.A. Montgomery Jr., J.E. Peralta, F. Ogliaro, M. Bearpark, J.J. Heyd, E. Brothers, K.N. Kudin, V.N. Staroverov, R. Kobayashi, J. Normand, K. Raghavachari, A. Rendell, J.C. Burant, S.S. Iyengar, J. Tomasi, M. Cossi, N. Rega, J.M. Millam, M. Klene, J.E. Knox, J.B. Cross, V. Bakken, C. Adamo, J. Jaramillo, R. Gomperts, R.E. Stratmann, O. Yazyev, A.J. Austin, R. Cammi, C. Pomelli, J.W. Ochterski, R.L. Martin, K. Morokuma, V.G. Zakrzewski, G.A. Voth, P. Salvador, J.J. Dannenberg, S. Dapprich, A.D. Daniels, Ö. Farkas, J.B. Foresman, J.V. Ortiz, J. Cioslowski, D.J. Fox, Gaussian 09, Gaussian, Inc., Wallingford, CT, 2009.
[46] R.F.W. Bader, AIMPAC: A Set of Programs for the Theory of Atoms in molecules, McMaster University, Hamilton, Ontario, Canada L8S 4M1, 1994.
[47] C. Gatti, R. Bianchi, R. Destro, F. Merati, J. Mol. Struct. (THEOCHEM) 255 (1992) 409.
[48] B. Silvi, C. Gatti, J. Phys. Chem. A 104 (2000) 947.
[49] T. Lippman, J.R. Schneider, Acta Crystallogr., Sect. A 56 (2000) 575.
[50] G.R. Desiraju, T. Steiner, The Weak Hydrogen Bond, Oxford University Press, Oxford, 2001.
[51] L.J. Farrugia, D.S. Middlemiss, R. Sillanpää, P. Seppälä, J. Phys. Chem. A 112 (2008) 9050.
[52] A. Holladay, P. Leung, P. Coppens, Acta Crystallogr., Sect. A 39 (1983) 377.
[53] A.E. Reed, L.A. Curtiss, F. Weinhold, Chem. Rev. 88 (1988) 899.
[54] P. Pillet, M. Souhassou, C. Mathoniere, C. Lecomte, J. Am. Chem. Soc. 126 (2004) 1219.
[55] X. Fradera, M.A. Austen, R.F.W. Bader, J. Phys. Chem. A 103 (1999) 304.